p-ISSN 2089 – 0133 e-ISSN 2477-6416
URL : https://jurnal.uns.ac.id/ijap/article/view/75790

DOI : https://doi.org/10.13057/ijap.v13i2.75790

COMPRESSIBILITY EFFECTS ON TURBULENT HEAT TRANSFER OF NATURAL CONVECTION IN A SQUARE CAVITY

Rida Siti Nur'aini Mahmudah, Restu Widiatmono*, Denny Darmawan
Physics Study Program Universitas Negeri Yogyakarta, Yogyakarta, Indonesia
*restu@uny.ac.id

Received 01-07-2023, Revised 07-08-2023, Accepted 24-09-2023
Available Online 24-09-2023, Published Regularly October 2023

ABSTRACT

Heat transfer in turbulent flows is one of the essential topics in power plants and thermal-based engineering. This study aims to analyze the effects of density changes due to heat transfer in a turbulent environment—which is usually neglected because it can cause instability in a simulation. We simulate an available experimental case of turbulent heat transfer of air with OpenFOAM: one with an incompressible approach (no density change) and another with a compressible treatment. The simulation geometry is a 0.75×0.75 m^2 square cavity, where its left and right walls are kept at a temperature difference of 40 K. We compare and analyze the temperature, velocity, and turbulence kinetic energy profiles of both simulation results against the experimental data. We found that from all qualitative and quantitative comparisons, the change in density plays a vital role in turbulent heat transfer. The compressible treatment gives better results than the incompressible: the neglection of density change causes a significant difference with the experimental data. Thus, we strongly recommended incorporating compressibility in simulating heat transfer in turbulent flows.

Keywords: heat transfer; OpenFOAM; square cavity; turbulent flow

Cite this as: Mahmudah, R. S. N., Widiatmono, R., & Darmawan, D. 2023. Compressibility Effects on Turbulent Heat Transfer of Naturan Convection in a Square Cavity. *IJAP: Indonesian Journal of Applied Science, 13*(2), 262-275. doi: https://doi.org/10.13057/ijap.v13i2.75790

INTRODUCTION

The study of heat transfer phenomena is of utmost importance in thermal engineering due to its widespread applications in various industrial and scientific fields. Specifically, heat transfer in turbulent conditions is the primary key technology in nowadays power plants that supply energy to the world. For example, it applies to heat exchangers [1–5] used by fossils, chemical power plants, and nuclear reactors [6]. In laminar flows, many studies [7–15] consider fluids undergoing heat transfer as incompressible, i.e., their density is constant regardless of their change in temperature and pressure. This assumption only applies if the temperature difference is below 2℃ for water and 15℃ for air [16]. Thus, other studies began considering the fluid's compressibility to the laminar flow [17–21].

On the other hand, when dealing with turbulent flows, compressibility can significantly influence the overall heat transfer characteristics. Compressibility effects arise due to variations in fluid density caused by changes in pressure and temperature, which lead to alterations in the thermodynamic and transport properties of the fluid. These effects become particularly pronounced when dealing with high-speed flows or when the Mach number of the flow exceeds a critical value. For air without undergoing heat transfer, one can ignore the compressibility

effect when the Mach number is less than 0.3[22–24]. However, when the flows involve heat transfer, it might be wise to consider the density changes regardless of the low Mach number.

Several studies show that the incorporation of weak compressibility[25] and "full" compressibility [26] in turbulent flow are more accurate than that of the incompressible in the case of pump and intercooler heat exchangers. Thus, we hypothesized that it is also essential to incorporate compressibility for turbulent heat transfer of air in a square cavity.

Several computational fluid dynamics codes have been used to simulate turbulent natural convection, such as OpenFOAM [27], Star-CCM+ [28], and ANSYS Fluent [29-30]. Among those, OpenFOAM [31] is the only free-of-charge software that has been used widely in numerous studies [32].

This study aims to prove our hypothesis by simulating the natural convection as incompressible and compressible flows with OpenFOAM. We solved each simulation with a different solver: buoyantBuossinesqSimpleFoam for incompressible and buoyantSimpleFoam for compressible flow. The turbulence model, grid size, initial and boundary conditions, and simulation algorithms are the same for both cases to see the results differences solely due to the compressibility. We compared both simulation results with the experimental data provided by [33] to analyze their differences in temperature, velocity, and turbulent kinetic energy.

METHOD

Governing Equations

The mass, momentum, and energy conservation equations govern fluid movement and interactions. In a steady-state turbulent flow, the first two equations, respectively, can be written as follows:

$$\nabla \cdot (\rho \boldsymbol{u}) = 0 \tag{1}$$

$$\frac{\partial(\rho \boldsymbol{u})}{\partial t} \nabla \cdot (\rho \boldsymbol{u}\boldsymbol{u}) = -\nabla p + \rho \boldsymbol{g} + \nabla \cdot \left(2\mu_{eff} D(\boldsymbol{u})\right) - \nabla \left(\frac{2}{3}\mu_{eff}(\nabla \cdot \boldsymbol{u})\right) \tag{2}$$

Where $\boldsymbol{u}$ is the velocity field, ρ is the density, p is the static pressure, and $\boldsymbol{g}$ is the gravitational acceleration. The effective viscosity μ_{eff} is the sum of turbulence μ_t and dynamic viscosity μ, and $D(\boldsymbol{u})$ is the rate of deformation tensor, defined as:

$$D(\boldsymbol{u}) = \frac{1}{2}(\nabla \boldsymbol{u} + (\nabla \boldsymbol{u})^T) \tag{3}$$

OpenFOAM determines the pressure gradient and gravity force terms in Equation (2) as Equation (4):

$$\begin{aligned} -\nabla p + \rho \boldsymbol{g} &= -\nabla\left(p_{rgh} + \rho \boldsymbol{g} \cdot \boldsymbol{r}\right) + \rho \boldsymbol{g} \\ &= -\nabla p_{rgh} - (\boldsymbol{g} \cdot \boldsymbol{r})\nabla \rho - \rho \boldsymbol{g} + \rho \boldsymbol{g} \\ &= -\nabla p_{rgh} - (\boldsymbol{g} \cdot \boldsymbol{r})\nabla \rho \end{aligned} \tag{4}$$

where p_{rgh} is the hydrostatic pressure, $p_{rgh} = p - \rho \boldsymbol{g} \cdot \boldsymbol{r}$, and $\boldsymbol{r}$ is the position vector. Equations (1) – (2) are solved in OpenFOAM's compressible flow solvers, such as buoyantSimpleFoam, employed in this study.

When the density is not constant, such as due to the change in temperature and pressure, one usually applies the Boussinesq approximation—to consider it constant, which is valid when the density variation is slight [16]. Here, we introduce reference density ρ_0 at a reference temperature T_0, and calculate density as:

$$\rho \approx \rho_0[1 - \beta(T - T_0)] \tag{5}$$

With β is the thermal expansion coefficient. After several mathematics manipulations, the momentum conservation Equation (2) for incompressible flows is:

$$\frac{\partial \boldsymbol{u}}{\partial t}\nabla \cdot (\boldsymbol{uu}) = -\nabla p_{rgh} - (\boldsymbol{g} \cdot \boldsymbol{r})\nabla\left(\frac{\rho}{\rho_0}\right) + \nabla \cdot \left(2\nu_{eff} D(\boldsymbol{u})\right) \tag{6}$$

where $\nu_{eff} = \mu_{eff}/\rho_0$ is the effective kinematic viscosity. Eqs. (1) and (6) are solved in OpenFOAM by incompressible flow solvers. Since this study aims to analyze the effect of compressibility, we used buoyantBoussinesqSimpleFoam as the incompressible flow solver because it only differs by applying the Boussinesq approximation from `buoyantSimpleFoam`. Thus, any results differences between the two solvers would be only due to the difference in density change treatment.

Heat Transfer

Simulation of heat transfer is performed by solving the energy equation. In this study, we chose the sensible enthalpy model of the buoyantSimpleFoam solver, which solved the following equation.

$$\nabla \cdot (\rho \boldsymbol{u} h) + \frac{\partial(\rho K)}{\partial t} + \nabla \cdot (\rho \boldsymbol{u} K) - \frac{\partial p}{\partial t} = \nabla \cdot \left(2\alpha_{eff}\nabla h\right) + \rho \boldsymbol{u} \cdot \boldsymbol{g} \tag{7}$$

The enthalpy per unit mass h is the sum of energy per unit mass e and kinematic pressure, $h = e + p/\rho$. $K \equiv |\boldsymbol{u}|^2/2$ is the kinetic energy per unit mass, and α_{eff}/ρ is the effective thermal diffusivity, defined as:

$$\alpha_{eff} = \frac{\rho \nu_t}{Pr_t} + \frac{\mu}{Pr} = \frac{\rho \nu_t}{Pr_t} + \frac{k}{c_p} \tag{8}$$

Where k is the thermal conductivity, c_p is the specific heat at constant pressure, Pr is the Prandtl number. For constant density approximation and with several mathematics manipulations, Equation (7) becomes:

$$\nabla \cdot (T\boldsymbol{u}) = k_{eff}\nabla^2 T \tag{9}$$

where $k_{eff} = k + k_t = \frac{\nu_0}{Pr} + \frac{\nu_t}{Pr_t}$. buoyantBoussinesqSimpleFoam solved Equation (9) to simulate the incompressible heat transfer flows.

Simulation geometry and setup

To validate the results, we simulate the existing experimental results of natural convection in a square cavity [33]. Figure 1 shows the experiment geometry in 2D.

In the experiment, the hot and cold was kept at isothermal condition with the temperature of $T_h = 50$°C and $T_c = 10$°C, respectively, resulting in a Rayleigh number of 1.58×10^9. Natural convection occurs when the air near the hot wall of the square cavity becomes warmer and

moves towards the cold wall, and vice versa. The experiment setup ensured the turbulent flow inside the cavity, with the turbulent parameters listed in Table 1. We used the same values in the simulation to reproduce the experimental results.

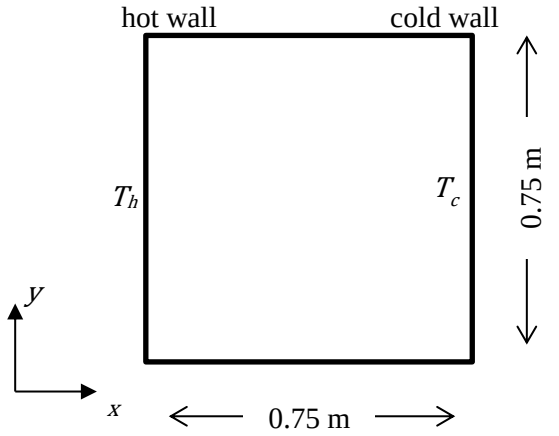

Figure 1. Simulation geometry

Table 1. Turbulent parameters

Parameter	Symbol	Value
Turbulence length scale	l	5 mm
Turbulence dissipation rate	ε	10^{-2} m^2/s^3
Turbulence kinetic energy	κ	4.5×10^{-3} m^2/s^2
Prandtl number	Pr	0.71
Turbulence Prandtl number	Pr_t	0.85
Empirical constant	C_μ	0.09 [34]

The simulations were performed by building the same geometry as the experiment (Figure 1), setting the initial and boundary conditions, and other parameters related to the model used. Table 2 lists the simulation setup, while Table 3 shows both simulations' initial and boundary conditions.

Table 2. Simulation set up

Parameter	Flow type	
	incompressible	compressible
algorithms	SIMPLE [35]	SIMPLE
turbulent model	$k-\omega$ SST [36,37]	$k-\omega$ SST
heat transfer model	Boussinesq approximation, $\beta = 3.34 \times 10^{-3}$/K	compressible
wall distance calculation	mesh-wave	mesh-wave
solver	buoyantBoussinesqSimpleFoam	buoyantSimpleFoam

After we set the simulation correctly, we run the simulation using the solver command: buoyantSimpleFoam for compressible flows and buoyantBoussinesqSimpleFoam for incompressible flows. There needs to be more information on how long the authors performed

the experiments. Assuming a steady state condition in the experiments, we run both cases until iteration steps of 20000, ensuring the steady state condition in the simulation. After running the simulations, we compare the results from both with the experiment's results of temperature, velocity, and turbulence kinetic energy κ quantitatively. Unfortunately, there are no qualitative results from the experiment; thus, we can only compare the qualitative results between the two solvers' results.

Table 3. Initial and boundary conditions

Properties	Initial condition	Boundary condition
Temperature (K)	323.15 at the hot wall, 283.15 at the cold wall, 303.15 at the rest of the domain	Isothermal at hot and cold wall Zero gradients at the top and bottom wall
Velocity, $\boldsymbol{u}$ (m/s)	0	No slip
Pressure, p (Pa)	Uniform 10^5	Calculated
Hydrostatic pressure, p_{rgh} (Pa)	Uniform 10^5	Fixed flux
Turbulence kinematic viscosity, ν_t (m^2/s)	0	Kinematic viscosity k-wall function

RESULTS AND DISCUSSION

As mentioned before, the first step is to build the geometry of the square cavity by 0.75 m × 0.75 m^2. OpenFOAM is a 3D specialized simulator; thus, we set the width of the square as one unit to make it 2D. Figure 2 shows the resulting geometry. We divided the simulation geometry into several grids of the same size (Figure 2 left). At the simulation's initial, the temperature was set as the experimental conditions, as seen in Figure 2 right. The hot wall is coloured red (the highest temperature in all domains), the cold wall is coloured blue (the coldest), and we set the middle as the ambient temperature—coloured green.

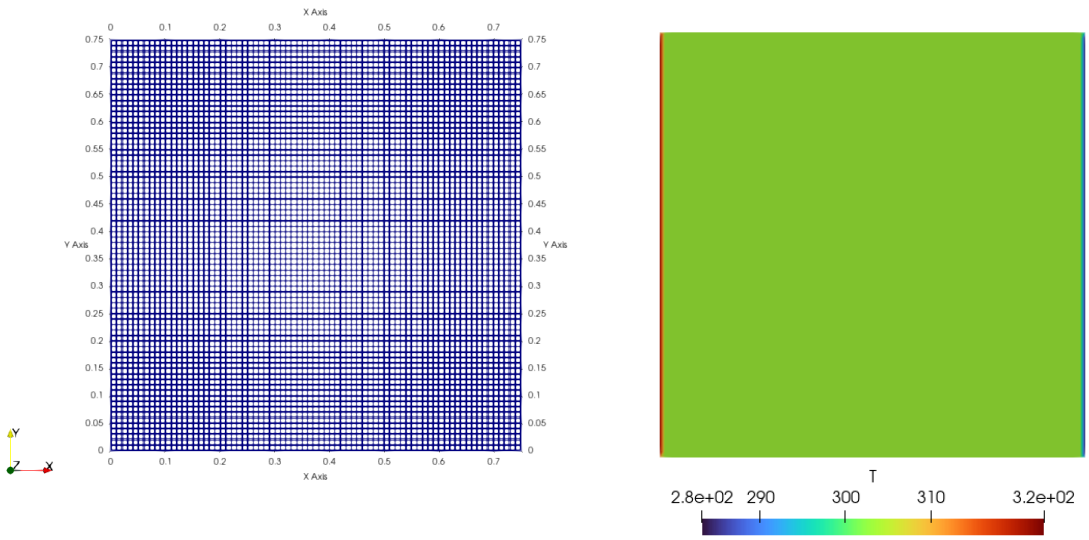

Figure 2. Grids in the simulation domain (left) and initial temperature setup (right)

After building the geometry and setting the initial and boundary conditions and the simulation parameters (Tables 2 and 3), we simulated with two different solvers. As soon as the simulation begins, the gravity force $\boldsymbol{g}$ (in the negative y-axis direction) and the heat transfer occur immediately. Both solvers solve the mass, momentum, and energy equations at each time step due to these changes by using the SIMPLE algorithm. They resulted in T, $\boldsymbol{u}$, p, and κ of every grid in each iteration. Figure 3 shows some of the visible temperature results from both solvers.

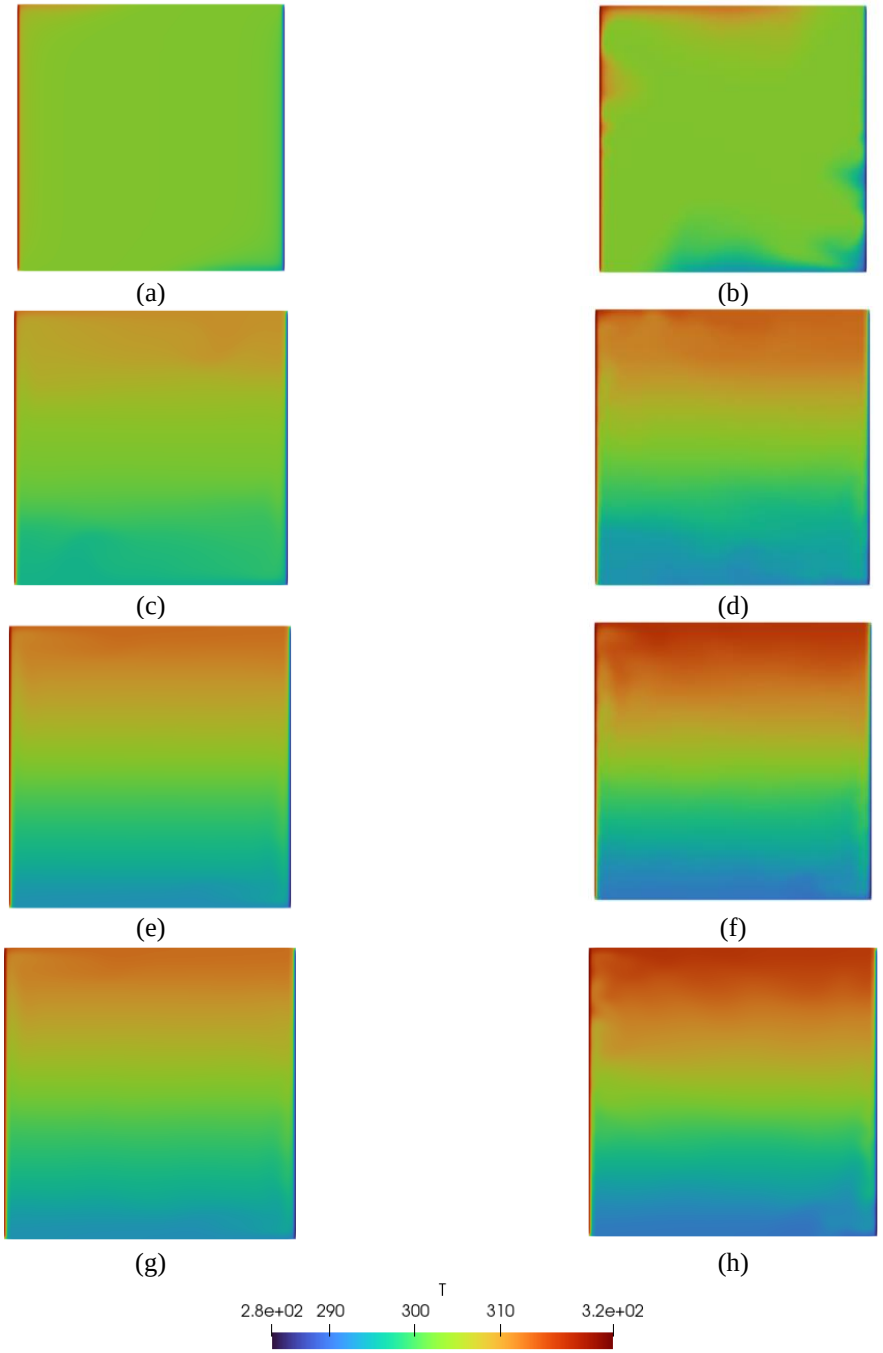

Figure 3. Temperature results, in Kelvin: (a) incompressible at 200 steps; (b) compressible at 200 steps; (c) incompressible at 1600 steps; (d) compressible at 1600 steps; (e) incompressible at 4000 steps; (f) compressible at 4000 steps; (g) incompressible at 20000 steps; (h) compressible at 20000 steps

As discussed before, as soon as the simulation run, air inside the cavity undergo heat transfer due to the temperature difference and experience gravity acceleration. Together, this will cause the air to move inside the cavity until it reaches the steady state condition. Air with a lower temperature will have higher density. Thus, air near the cold wall will start to move downward and get to the bottom wall, and as soon as it reaches the hot wall, its density begins to increase so that it will go upward along the hot wall.

On the other hand, the air near the hot wall will move upward due to the lower density. It then moves along the top border, and as soon as it reaches the cold wall, it begins to move downward. These phenomena can be seen in Figure 3 as the changing temperature. At 200 iteration steps—for example (Figure 3(a) and 3(b)), we can see the red spread to the upper left and the blue extended to the bottom right, describing the hot and cold air movement, respectively.

Figure 3 also shows visible differences between incompressible and compressible simulation results. Since iteration steps of 200, the heat transfer of the compressible flow (Figure 3(b)) seems to occur more rapidly than of the incompressible (Figure 3(a)), shown by the reddish at the top of the geometry and more blueish at the bottom. This tendency grew in every iteration and resulted in the faster construction of the three horizontal layers of red-green-blue in the compressible flow, which occurred since iteration steps of 1600 (Figure 3(d)). These layers are visible in the incompressible flow after iteration steps of 4000 (Figure 3(e)). Moreover, the visual temperature results show a sharper reddish and blueish colour, indicating more heat transfer in the compressible flow.

To determine which results are closer to real life, we compare both simulation results quantitatively with experimental data, as discussed below.

Compressibility effect on temperature

Figure 4 shows a temperature comparison of the experiment, the incompressible, and the compressible simulation results. Here, $Y = y/L$, where $L = 0.75$ m is the cavity's length. $Y = 0.5$ means we extract the data along $y = 0.375$ m, i.e., in the middle of the cavity's height. The plot is the dimensionless distance along the x-axis, $X = x/L$, against the dimensionless temperature $\frac{T-T_c}{\Delta T}$, where $\Delta T = T_h - T_c = 40$ K.

We can see from Figure 4 that simulation results with compressible treatment show better agreement with the experimental data than the incompressible. Both simulations can reproduce the experimental data well in the near hot and cold walls but differ significantly afterwards. We observed that the incompressible treatment underestimated the experiment results. $\frac{T-T_c}{\Delta T} = 0.5$ means that the temperature is the same as the ambient temperature, i.e., the moderate temperature between the hot and the cold walls, 30°C. For the incompressible flow, the average temperature in the middle of the cavity is lower than the ambient because it does not incorporate the density changes. Meanwhile, the compressible treatment changes the air density it will decrease with increasing temperature. Due to gravity, the lower density the hotter air will move faster, and the higher density the colder air will move slower. As time goes on and natural convection occurs continuously, the hotter air will overcome the colder air movement. Thus, it will dominate the cavity as seen in Figure 3 as redder making the temperature in the middle cavity slightly higher than the ambient in the compressible flows. We can also observe this phenomenon in the experiment.

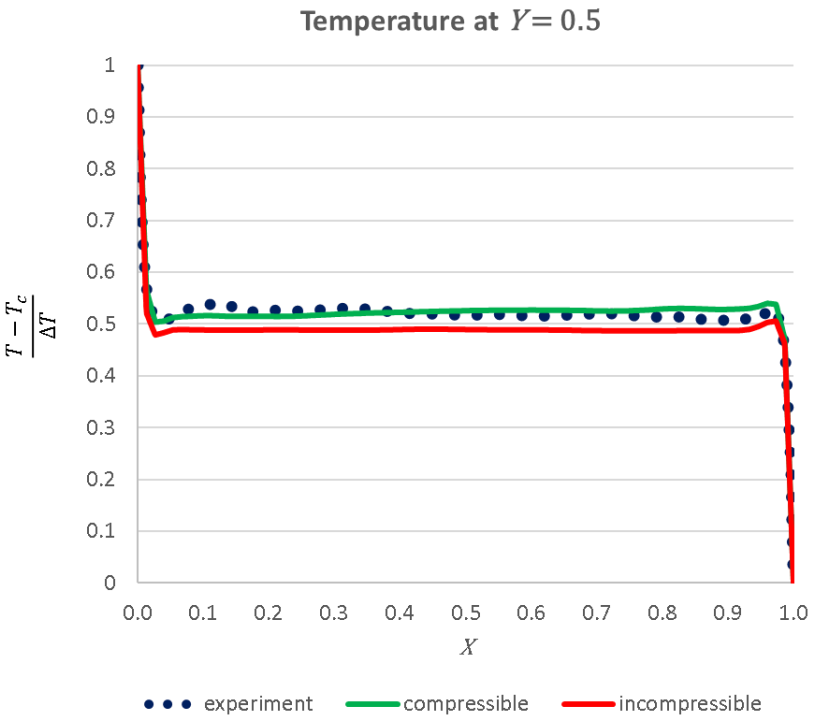

Figure 4. Temperature comparison

On the other hand, the incompressible treatment does not consider the changing density due to the temperature change. Thus, there is no considerable movement difference between the hot and cold air. They almost balanced each other, and the average temperature of the cavity was slightly lower than the ambient.

Compressibility effect on velocity

To analyze the air movement, we compare the experimental data of the air's vertical velocity with the simulation results. Figure 5 shows the dimensionless velocity profile at $Y = 0.5$, where v_y is the vertical velocity, and $V_0 = \sqrt{\boldsymbol{g}\beta L\Delta T} = 1$ m/s.

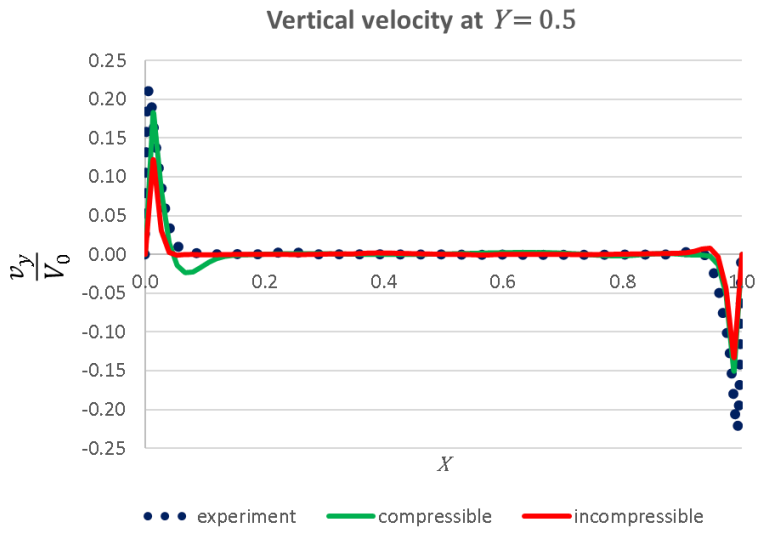

Figure 5. Velocity comparison

As expected, the air in the middle of the cavity is not moving, $\frac{v_y}{V_0} = 0$ because the air temperature there is the ambient temperature—no heat transfer occurs. Thus, there is no movement due to temperature changes. Near the walls, the air's velocity is high in the upward direction (the hot wall) and downward direction (the cold wall)—generally, the compressible treatment results in better agreement with the experimental data than the incompressible. As discussed, the air moves faster in the compressible treatment, resulting in higher velocity than in the incompressible treatment.

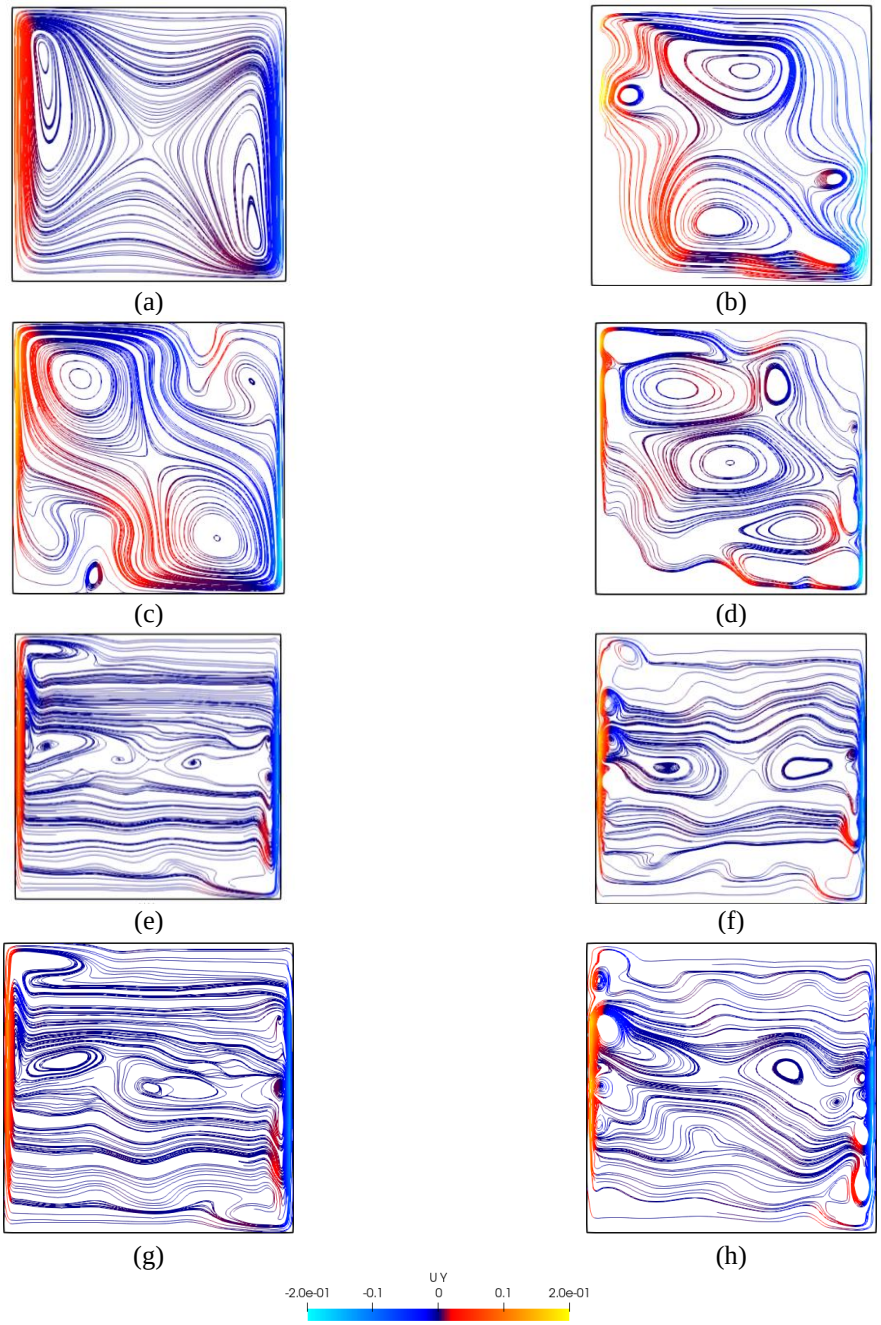

Figure 6. Vertical velocity profiles, in m/s: (a) incompressible at 200 steps; (b) compressible at 200 steps; (c) incompressible at 1000 steps; (d) compressible at 1000 steps; (e) incompressible at 10000 steps; (f) compressible at 10000 steps; (g) incompressible at 20000 steps; (h) compressible at 20000 steps

To analyze the difference further, we compare the qualitative results of vertical velocity streamlines from both simulations in Figure 6. For brevity, we limit the comparison to four iterations.

Figure 6 shows the significantly different vertical velocity profiles between the two solvers. It indicates a nearly symmetrical velocity profile of the incompressible treatment (Figure 6(a), (c), (e), and (g)). We only found this symmetrical profile in the early steps of the compressible treatment until the iteration steps of 200 (Figure 6(b)). After that, the velocity profile tends to be chaotic no visible symmetric pattern is observed. The chaotic pattern is due to the compressibility or the density changes, causing more flow fluctuations; thus, making it even more turbulent.

The symmetrical velocity profile is commonly found in laminar flows. In a turbulent flow, the fluid's velocity profile should be asymmetry, as has been seen by other studies [38-39]. Moreover, the compressible results show more eddies than the incompressible, other characteristics of turbulent flows. Thus, the compressible treatment can reproduce the features of the turbulent flow more than the incompressible.

Compressibility effect on kinetic turbulence energy

Lastly, we compare the experimental data of turbulence kinetic energy with both simulations. Here, turbulence kinetic energy κ is the total squared velocity fluctuations in all directions as defined by [40]. As in the previous discussions, we compare the profile at $Y = 0.5$; the results can be seen in Figure 7.

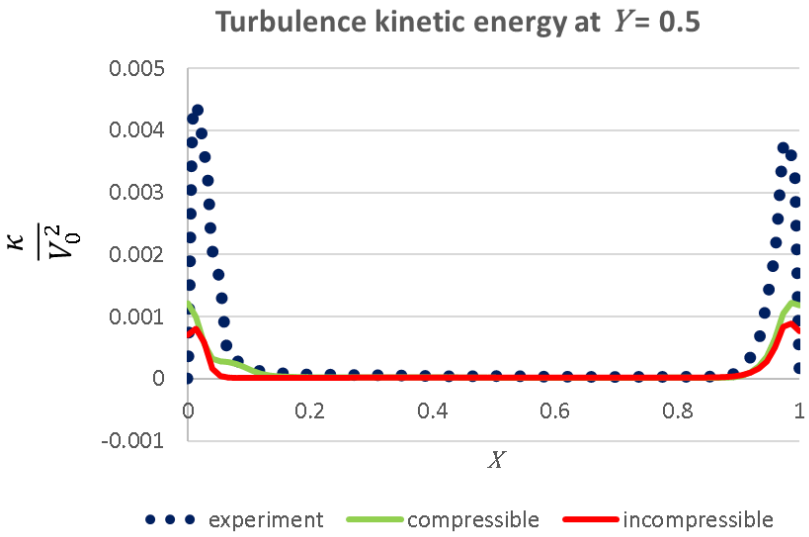

Figure 7. Turbulence kinetic energy comparison

Figure 7 shows good agreement between experimental data and simulations at $0.1 \leq X \leq 0.9$. However, both simulations underestimate the experimental data near the hot and cold walls. The turbulence kinetic energy is significantly higher than in other regions due to high-velocity fluctuations in the hottest and the coldest air. The authors suggest that this difference is due to the simulation's grid size—which due to the lack of computational resources at the time of this study, was set to 1 cm. We strongly believe that the simulation results can be improved with higher domain resolution, as found by [41-42]. Nonetheless, as the temperature and velocity comparison, the compressible treatment produces better agreement than the incompressible.

To further see the results difference between the two solvers, we plot the contour of the turbulence kinetic energy profile in Figure 8. Since the temperature profile between the two differs significantly in the earlier simulation (Figure 3), and for brevity, we focus our analysis of the turbulence kinetic energy until the iteration steps 1400.

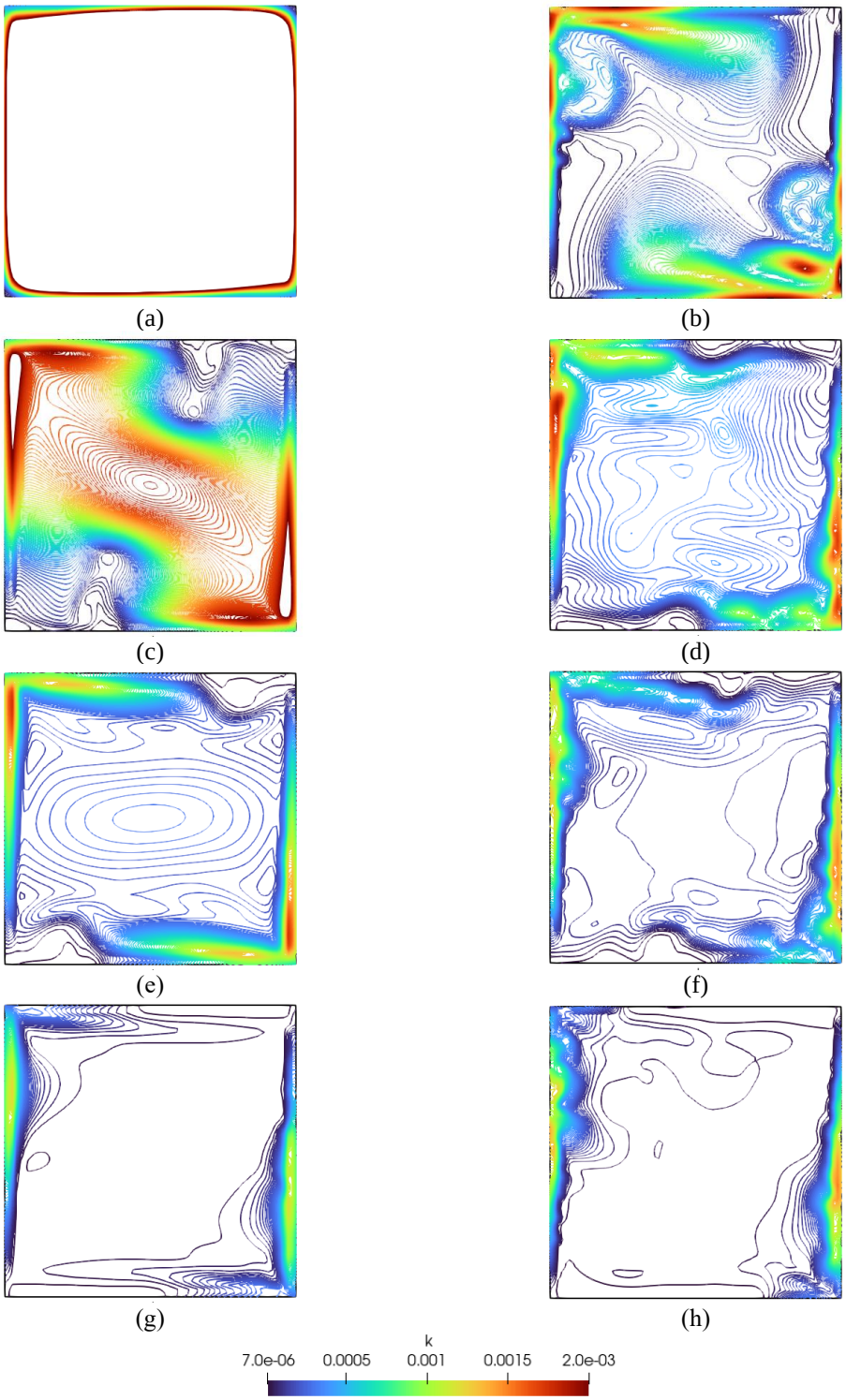

Figure 8. Turbulent kinetic energy contour, in J/kg: (a) incompressible at 200 steps; (b) compressible at 200 steps; (c) incompressible at 1000 steps; (d) compressible at 1000 steps; (e) incompressible at 1400 steps; (f) compressible at 1400 steps; (g) incompressible at 2400 steps; (h) compressible at 2400 steps

We observe a striking difference in the turbulent kinetic energy contour in Figure 8. Along with the faster air movement, the turbulent kinetic energy in the compressible flow increases and spreads faster throughout the cavity. Even as early as iterations steps of 200 (Figure 8(b)), we can see the turbulence phenomena in the compressible treatment. Meanwhile, in the incompressible treatment, the symmetrical profile of turbulent kinetic energy can be seen until iterations of 2400 (Figure 8(g)) before the air movement becomes chaotic. As time passes, the cavity's middle part results in zero turbulence kinetic energy due to the reaching of the steady state—ambient temperature. The contour comparison of turbulence kinetic energy strengthened our previous discussion about the effect of density changes on the flow's profile.

CONCLUSION

This study analyzes the compressibility effect on turbulent natural air convection in a square cavity. We performed the simulations using two different solvers of OpenFOAM: buoyantBuossinesqSimpleFoam for incompressible simulation and buoyantSimpleFoam for compressible simulation. We compared both simulation results with available experimental temperature, vertical velocity, and turbulence kinetic energy data. Based on qualitative and quantitative results, we concluded that the changes in density due to the temperature changes play a significant role in turbulent heat transfer. Incorporating the compressible effect is highly recommended when simulating heat transfer in a turbulent environment, even though the flow's Mach number is below 0.3. We recommend using a smaller grid size to get more accurate simulation results, especially near the hot and cold walls.

ACKNOWLEDGMENTS

The authors thank the Ministry of Education and Culture of Indonesia for their financial support, which was pivotal in completing this study. The funding was provided under the scheme of Fundamental Research of 2023, contract and sub-contract numbers: 146/E5/PG.02.00.PL/2023, and T/13.10 /UN34.9/PT.01.03/2023. This support facilitated the realization of our research objectives and strengthened our commitment to advancing knowledge in our field.

REFERENCES

1. Zhang, K., Sun, Z., Zheng, N., & Chen, Q. 2020. Effects of the configuration of winglet vortex generators on turbulent heat transfer enhancement in circular tubes. *International Journal of Heat and Mass Transfer*, *157*, 119928.
2. Zhang, S., Lu, L., Wen, T., & Dong, C. 2021. Turbulent heat transfer and flow analysis of hybrid Al2O3-CuO/water nanofluid: An experiment and CFD simulation study. *Applied Thermal Engineering*, *188*, 116589.
3. Ajarostaghi, S. S. M., Zaboli, M., & Nourbakhsh, M. 2021. Numerical evaluation of turbulence heat transfer and fluid flow of hybrid nanofluids in a pipe with innovative vortex generator. *Journal of Thermal Analysis and Calorimetry*, *143*, 1583-1597.
4. Omidi, M., Rabienataj Darzi, A. A., & Farhadi, M. 2019. Turbulent heat transfer and fluid flow of alumina nanofluid inside three-lobed twisted tube. *Journal of Thermal Analysis and Calorimetry*, *137*, 1451-1462.

5. Yu, C., Zhang, H., Zeng, M., Wang, R., & Gao, B. 2020. Numerical study on turbulent heat transfer performance of a new compound parallel flow shell and tube heat exchanger with longitudinal vortex generator. *Applied Thermal Engineering*, *164*, 114449.
6. Shams, A., De Santis, A., Koloszar, L. K., Ortiz, A. V., & Narayanan, C. 2019. Status and perspectives of turbulent heat transfer modelling in low-Prandtl number fluids. *Nuclear Engineering and Design*, *353*, 110220.
7. Lee, J. H., Shin, J. H., Chang, S. M., & Min, T. 2020. Numerical analysis on natural convection heat transfer in a single circular fin-tube heat exchanger (Part 1): numerical method. *Entropy*, *22*(3), 363.
8. Lahmer, E. B., Moussaoui, M. A., & Mezrhab, A. 2019. Investigation of laminar flow and convective heat transfer in a constricted channel based on double MRT-LBM. In *2019 International Conference on Wireless Technologies, Embedded and Intelligent Systems (WITS)*, 1-6. IEEE.
9. Mostafavi, A., & Jain, A. 2022. Theoretical analysis of unsteady convective heat transfer from a flat plate with time-varying and spatially-varying temperature distribution. *International Journal of Heat and Mass Transfer*, *183*, 122061.
10. Laouira, H., Mebarek-Oudina, F., Hussein, A. K., Kolsi, L., Merah, A., & Younis, O. 2020. Heat transfer inside a horizontal channel with an open trapezoidal enclosure subjected to a heat source of different lengths. *Heat Transfer—Asian Research*, *49*(1), 406-423.
11. Adhikari, S. C., Hasan, M. S., Akter, R., & Nath, R. 2021. Unsteady Features of Laminar Viscous Incompressible Flow and Temperature Dissemination through a Rotating Bent Rectangular Channel: The Case of Negative Rotation. *Jagannath University Journal of Science*, *8*(1), 33-44.
12. Razera, A. L., Quezada, L. A., Fagundes, T. M., Isoldi, L. A., dos Santos, E. D., Biserni, C., & Rocha, L. A. O. 2019. Fluid flow and heat transfer maximization of elliptic cross-section tubes exposed to forced convection: A numerical approach motivated by Bejan's theory. *International Communications in Heat and Mass Transfer*, *109*, 104366.
13. Belhocine, A., Stojanovic, N., & Abdullah, O. I. 2021. Numerical simulation of laminar boundary layer flow over a horizontal flat plate in external incompressible viscous fluid. *European Journal of Computational Mechanics*, 337-386.
14. Menni, Y., Chamkha, A., Zidani, C., & Benyoucef, B. 2020. Baffle orientation and geometry effects on turbulent heat transfer of a constant property incompressible fluid flow inside a rectangular channel. *International Journal of Numerical Methods for Heat & Fluid Flow*, *30*(6), 3027-3052.
15. El Desouky, A. A., Ismail, H. N. A., Abourabia, A. M., & Ahmed, N. A. 2020. Numerical simulation of MHD flow and heat transfer inside T-shaped cavity by the parallel walls motion. *SN Applied Sciences*, *2*, 1-18.
16. Ferziger JH, Perić M. 2012. *Computational Methods for Fluid Dynamics*. 3rd ed. Springer Berlin Heidelberg.
17. Vila-Pérez, J., Giacomini, M., & Huerta, A. 2023. Benchmarking the face-centred finite volume method for compressible laminar flows. *International Journal of Numerical Methods for Heat & Fluid Flow*, *33*(6), 2198-2231..
18. Cavazzuti, M. 2020. Viscous heating effects on heat transfer characteristics of laminar compressible channel flow. *International Journal of Heat and Mass Transfer*, *153*, 119608.
19. Saini, D., & Sandberg, R. D. 2020. Simulations of compressibility effects in centrifugal buoyancy-induced flow in a closed rotating cavity. *International Journal of Heat and Fluid Flow*, *85*, 108656.
20. Ren, B., Li, C. G., & Tsubokura, M. 2021. Laminar natural convection in a square cavity with 3D random roughness elements considering the compressibility of the fluid. *International Journal of Heat and Mass Transfer*, *173*, 121248.
21. Zhao, B. 2021. Derivation of unifying formulae for convective heat transfer in compressible flow fields. *Scientific Reports*, *11*(1), 16762.
22. Guo, Z., Liu, H., Luo, L. S., & Xu, K. 2008. A comparative study of the LBE and GKS methods for 2D near incompressible laminar flows. *Journal of Computational Physics*, *227*(10), 4955-4976.

23. Matsuyama, S. 2014. Performance of all-speed AUSM-family schemes for DNS of low Mach number turbulent channel flow. *Computers & Fluids*, *91*, 130-143.
24. Weigand, B., & Mitra, N. K. 2010. *VDI Heat Atlas.*
25. Zhang, F., Li, N., Zhu, D., Xiao, R., Liu, W., & Tao, R. 2022. Influence of weak compressibility on the hydrodynamic performance evaluation of pump turbines in the pump mode. *Science and Technology of Nuclear Installations*, *2022*.
26. Yu, C., Qin, S., Chai, B., Huang, S., & Liu, Y. 2019. The Effect of Compressible Flow on Heat Transfer Performance of Heat Exchanger by Computational Fluid Dynamics (CFD) Simulation. *Entropy*, *21*(9), 829.
27. Logie, W. R., Abbasi-Shavazi, E., Hughes, G., & Pye, J. D. 2017. Turbulent contribution to heat loss in cavity receivers. In *AIP Conference Proceedings*, 1850(1). AIP Publishing.
28. Freile, R., Tano, M., Balestra, P., Schunert, S., & Kimber, M. 2021. Improved natural convection heat transfer correlations for reactor cavity cooling systems of high-temperature gas-cooled reactors: From computational fluid dynamics to Pronghorn. *Annals of Nuclear Energy*, *163*, 108547.
29. Voronina, A. V., & Pavlov, S. V. 2021. Selection of a turbulence model to calculate the temperature profile near the surface of VVER-1000 fuel assemblies in the NPP spent fuel pool. *Nuclear Energy and Technology*, *7*(2), 79-84.
30. Babanezhad, M., Behroyan, I., Nakhjiri, A. T., Rezakazemi, M., Marjani, A., & Shirazian, S. 2021. Thermal prediction of turbulent forced convection of nanofluid using computational fluid dynamics coupled genetic algorithm with fuzzy interface system. *Scientific Reports*, *11*(1), 1308.
31. Jasak, H. 2009. OpenFOAM: Open source CFD in research and industry. *International Journal of Naval Architecture and Ocean Engineering*, *1*(2), 89-94.
32. Chen, G., Xiong, Q., Morris, P. J., Paterson, E. G., Sergeev, A., & Wang, Y. 2014. OpenFOAM for computational fluid dynamics. *Notices of the AMS*, *61*(4), 354-363.
33. Ampofo, F., & Karayiannis, T. G. 2003. Experimental benchmark data for turbulent natural convection in an air filled square cavity. *International Journal of Heat and Mass Transfer*, *46*(19), 3551-3572.
34. Launder, B. E., & Sharma, B. I. 1974. Application of the energy-dissipation model of turbulence to the calculation of flow near a spinning disc. *Letters in heat and mass transfer*, *1*(2), 131-137.
35. Caretto, L. S., Gosman, A. D., Patankar, S. V., & Spalding, D. B. 1973. Two calculation procedures for steady, three-dimensional flows with recirculation. *Proceedings of the Third International Conference on Numerical Methods in Fluid Mechanics, 2*, 60-68.
36. Menter, F. R., Kuntz, M., & Langtry, R. (2003). Ten years of industrial experience with the SST turbulence model. *Turbulence, heat and mass transfer*, *4*(1), 625-632.
37. Menter, F. R. 1994. Two-equation eddy-viscosity turbulence models for engineering applications. *AIAA journal*, *32*(8), 1598-1605.
38. Livescu, D. 2020. Turbulence with large thermal and compositional density variations. *Annual Review of Fluid Mechanics*, *52*, 309-341. https://doi.org/101146/annurev-fluid-010719-060114
39. Zimmermann, C., & Groll, R. 2014. Modelling turbulent heat transfer in a natural convection flow. *Journal of applied mathematics and physics*, *2014*.
40. Pope SB. 2000. *Turbulent Flows.* Cambridge University Press.
41. Bahatmaka, A., Kim, D. J., & Zhang, Y. 2018. Verification of CFD method for meshing analysis on the propeller performance with OpenFOAM. In *2018 International Conference on Computing, Electronics & Communications Engineering (iCCECE)* (pp. 302-306). IEEE.
42. Larsen, B. E., Fuhrman, D. R., & Roenby, J. 2019. Performance of interFoam on the simulation of progressive waves. *Coastal Engineering Journal*, *61*(3), 380-400.